The *Swift* X-Ray Telescope

David N. Burrows[*a], J. E. Hill[a], J. A. Nousek[a] , A. Wells[b], G. Chincarini[c], A. F. Abbey[b], A. Beardmore[b], J. Bosworth[f], H. W. Bräuninger[d], W. Burkert[d], S. Campana[c], M. Capalbi[e], W. Chang[f], O. Citterio[c], M. J. Freyberg[d], P. Giommi[e], G. D. Hartner[d], R. Killough[g], B. Kittle[f], R. Klar[g], C. Mangels[g], M. McMeekin[f], B.J. Miles[a], A. Moretti[c], K. Mori[a], D. C. Morris[a], K. Mukerjee[b], J. P. Osborne[b], A.D.T. Short[b], G. Tagliaferri[c], F. Tamburelli[e], D. J. Watson[b], R. Willingale[b], M. Zugger[a]

[a]Pennsylvania State University, 525 Davey Lab, University Park, PA 16802, USA
[b]Space Research Centre, University of Leicester, Leicester LE1 7RH, UK
[c]Osservatorio Astronomico di Brera, Via Brera 28, 20121 Milano, Italy
[d]Max-Planck-Institut für Extraterrestrische Physik, Garching bei München, Germany
[e]ASI Science Data Center, Frascati, Italy
[f]Swales Aerospace, Inc., [g]Southwest Research Institute

ABSTRACT

The Swift Gamma-Ray Explorer is designed to make prompt multiwavelength observations of Gamma-Ray Bursts (GRBs) and GRB Afterglows. The X-ray Telescope (XRT) provides key capabilities that permit Swift to determine GRB positions with a few arcseconds accuracy within 100 seconds of the burst onset.

The *XRT* utilizes a superb mirror set[1] built for *JET-X*[2] and a state-of-the-art *XMM/EPIC MOS* CCD detector[3,4] to provide a sensitive broad-band (0.2-10 keV) X-ray imager with effective area of 135 cm^2 at 1.5 keV, field of view of 23.6 x 23.6 arcminutes, and angular resolution of 18 arcseconds (HEW). The detection sensitivity is $2x10^{-14}$ $erg/cm^2/s$ in 10^4 seconds. The instrument is designed to provide automated source detection and position reporting within 5 seconds of target acquisition. It can also measure redshifts of GRBs for bursts with Fe line emission or other spectral features. The *XRT* will operate in an auto-exposure mode, adjusting the CCD readout mode automatically to optimize the science return for each frame as the source fades. The *XRT* will measure spectra and lightcurves of the GRB afterglow beginning about a minute after the burst and will follow each burst for days as it fades from view.

Keywords: gamma-ray burst, X-ray telescope, Swift, X-ray instrumentation, X-ray CCD detector, X-ray mirrors

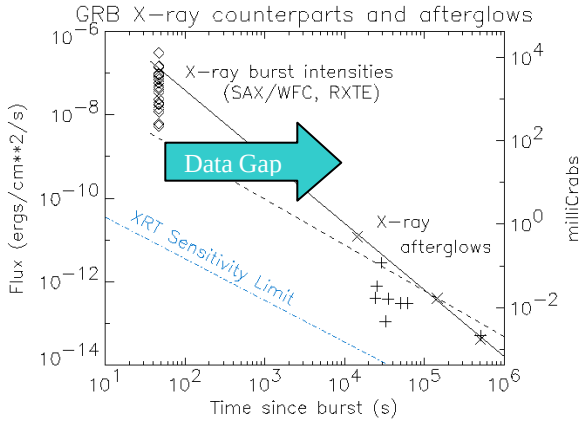

Fig. 1: X-ray burst and afterglow lightcurves. The cluster of data points at about 1 minute represents peak X-ray burst fluxes for a number of bursts observed by *Beppo-SAX* and *RXTE*. The data points between 10^4 and 10^6 seconds after the burst are *Beppo-SAX*, *RXTE*, and *ASCA* afterglow flux measurements. Note the data gap of about 10^4 seconds, during which the afterglow flux drops by about 4 orders of magnitude. The *Swift XRT* will fill in this data gap.

1 INTRODUCTION

The *Swift* Gamma Ray Burst Explorer[5] was chosen in October 1999 as the next MIDEX mission, with launch now scheduled in early 2004. It carries three instruments: a *Burst Alert Telescope (BAT* [6]*)*, which identifies gamma-ray bursts (GRBs) and determines their location on the sky to within a few arcminutes; an *Ultraviolet/Optical Telescope (UVOT* [7]*)* with sensitivity down to 24th magnitude and 0.3 arcsecond positions; and an *X-ray Telescope* (*XRT*). The three instruments combine to make a powerful multiwavelength observatory with the capability of rapid position determinations of GRBs to arcsecond accuracy within 1-2 minutes of their discovery, and the ability

* burrows@astro.psu.edu; phone 1 (814) 865-7707; fax 1 (814) 865-9100; http://www.swift.psu.edu/xrt

to measure both lightcurves and redshifts of the bursts and afterglows.

The *Swift XRT* is a sensitive, flexible, autonomous X-ray imaging spectrometer designed to measure fluxes, spectra, and lightcurves of GRBs and afterglows over a wide dynamic range of more than 7 orders of magnitude in flux. The *Beppo-SAX* satellite showed that accurate GRB positions can be effectively determined by a good X-ray telescope, since over 84% of GRBs have X-ray afterglows[12], compared with about 50% for optical afterglows. However, by the time that *Beppo-SAX* was able to observe a typical X-ray afterglow, its intensity had already dropped by 4-5 orders of magnitude (Fig. 1). The *Swift XRT* will begin observations before the GRB ends in many cases, and will fill in the large time gap during which the Lorenz factor of the relativistic blast wave changes from ~100 to <10. It will provide accurate positions within 5 seconds of target acquisition for typical bursts, allowing ground-based optical telescopes to begin immediate spectroscopic observations of the afterglow.

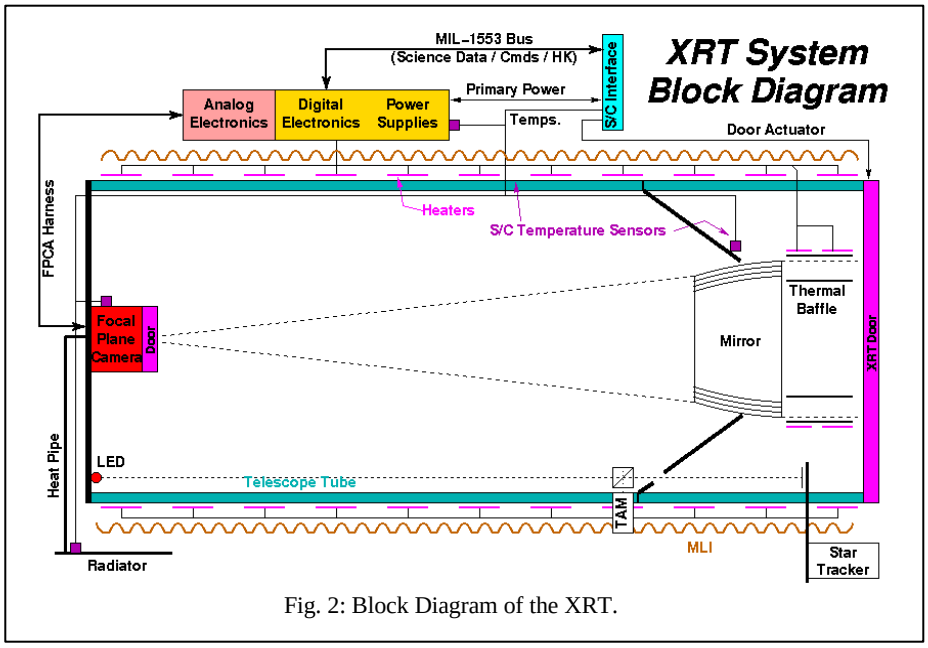

Fig. 2: Block Diagram of the XRT.

We previously reported on the instrument design at an early stage in its development[15]. Here we describe the final design and performance of the *XRT*.

2 OVERALL DESCRIPTION

The *XRT* uses a grazing incidence Wolter I telescope to focus X-rays onto an *XMM/EPIC MOS* CCD. The layout of the instrument is shown in Figures 2 and 3. Figure 4 is a photo of the completed instrument (before MLI installation). A door protects the mirrors during launch. Thermal baffles provide a warm environment for the front end of the mirrors and prevent any thermal gradients across them from distorting the Point Spread Function (PSF). The mirrors are the *JET-X*[1,2,8] flight spares, and were calibrated at the Panter X-ray Calibration Facility of the Max-Planck-Institute für Extraterrestrische Physik in 1996[1] and again in July 2000. A composite telescope tube holds the focal plane camera, which contains a single CCD-22 detector. A thermal radiator mounted on the anti-solar side of the spacecraft is coupled to a Peltier cooler that cools the detector to -100 C.

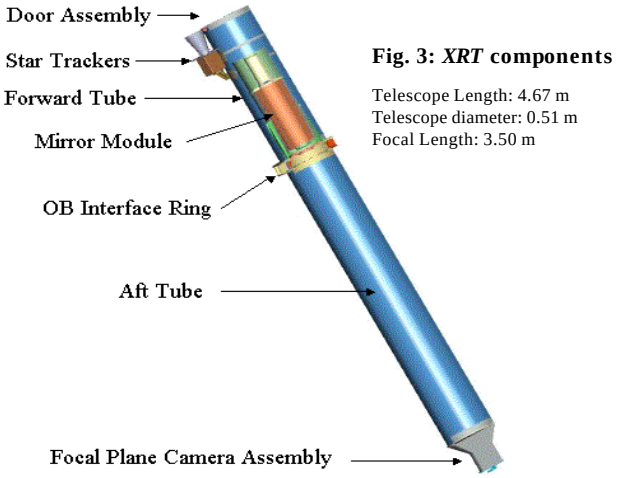

Fig. 3: *XRT* components

Telescope Length: 4.67 m
Telescope diameter: 0.51 m
Focal Length: 3.50 m

Table 1 gives the basic design parameters of the *XRT*. The effective area and sensitivity have been verified by an end-to-end X-ray calibration of the assembled instrument at the Panter X-ray calibration facility in September 2002.

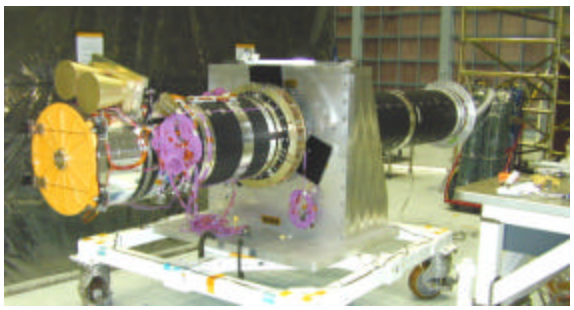
Fig. 4: *XRT* installed in GSE cart before thermal vacuum tests in July 2002, with star tracker simulators installed.

Table 1: *XRT* instrument characteristics

Telescope	3.5m Wolter I
Telescope PSF	18 arcsec HPD @ 1.5 keV 22 arcsec HPD @ 8.1 keV
Detector	MAT CCD-22
Detector Format	600 x 602 pixels
Detector Readout Modes	Photon-counting, Imaging, & Timing
Field of View	23.6 x 23.6 arcmin
Pixel Scale	2.36 arcsec / pixel
Energy Range	0.2 - 10 keV
Effective Area	135 cm^2 @ 1.5 keV
Sensitivity	2 x 10^{-14} ergs/cm^2/s in 10^4 s
Position Accuracy	2.5 arcseconds
Operation	Autonomous

Figure 5 is a photograph of the *XRT* installed in the *Swift* spacecraft. The design and scientific capabilities of the instrument are summarized in the following sections.

3 SCIENCE REQUIREMENTS

There are three primary requirements that drive the design of the *XRT*: rapid, accurate positions, moderate resolution spectroscopy, and high time resolution lightcurves.

GRB Position Determination: The *XRT* is required to measure afterglow positions with uncertainty of less than 5 arcseconds within 100 s of a burst alert from the *BAT*, which provides a GRB position accurate to about 4 arcminutes. The spacecraft will slew to the BAT position in 20-75 s, depending on the position of the GRB on the sky. Figure 6 shows a simulated *XRT* image of a GRB, made using raytracing code developed for *JET-X* and *Beppo-SAX* and incorporating the measured Point Spread Function (PSF) of the *XRT* mirrors. The mirror PSF has a 15 arcsecond Half-Energy Width (HEW) at the best on-axis focus (at 1.5 keV). It is slightly defocused in the *XRT* in order to provide a more uniform PSF over the entire field of view, and the instrument PSF is 18 arcseconds (HEW) at 1.5 keV[9]. The centroid of a point source image can be determined to sub-arcsecond accuracy in detector coordinates, given sufficient photons[10]. Based on *Beppo-SAX* and *RXTE* observations of X-ray counterparts of GRBs, we expect that most GRBs observed by *Swift* will have prompt X-ray fluxes of roughly 0.5 - 5 Crabs in the 0.2-10 keV band (Figure 1). *XRT* calibration data show that the *XRT* will obtain source positions to 1-3 arcseconds in detector coordinates for typical afterglows within 5 seconds of target acquisition.

Fig. 5: *Swift* observatory with Narrow Field Instruments installed. The *XRT* is the left-hand telescope tube. The white box to the left of the person is the *XRT* electronics.

When this position is referenced back to the sky, the expected error is 3-5 arcseconds, with the increase due primarily to the alignment uncertainty between the star

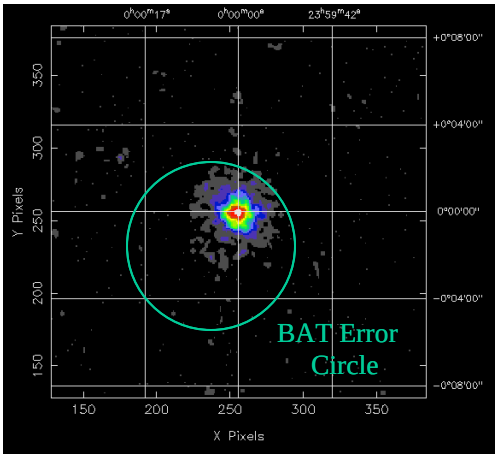

Fig. 6: Simulation of 100 s *XRT* observation, using the measured PSF of the *XRT* mirrors. The BAT error circle (4 arcminutes) is overlaid for comparison.

tracker and the *XRT*. In order to minimize this error term, the star trackers are mounted on the *XRT* forward telescope tube (Figures 3, 4), and a Telescope Alignment Monitor (TAM) measures flexing of the telescope tube with subarcsecond accuracy.

Spectroscopy: X-ray spectroscopy will provide important information on the GRB/afterglow properties. In the standard fireball model, the GRB is produced by internal shocks in the relativistic fireball and the afterglow is produced by external shocks with the ambient medium. While most of the X-ray luminosity of the afterglows arises from non-thermal synchrotron emission from the external shock, there have been reports of X-ray line emission from GRB afterglows[18,19]. These may be the result of thermal emission or X-ray reflection. Observations of the X-ray spectrum may therefore detect emission lines, which can provide direct information on such parameters as the composition and ionization structure of the shocked gas, as well as the redshift of the GRB source. Absorption edges from surrounding unshocked gas will be observable over a wide range of column densities, and these edges can also provide both redshift and abundance information.

The *XRT* energy resolution at launch will be about 135 eV at 6 keV (Figure 15), and spectra similar to that shown in Figure 7 will be obtained routinely. The strong Fe emission line in this simulated spectrum (E_{rest}=6.4 keV) enables a measurement of the redshift that is accurate to about 10%. The resolution will degrade during the mission, but remains better than 300 eV at end of life for a worst-case radiation environment. We will transmit spectra to the ground through our TDRSS link within 5-10 minutes of each BAT burst alert to facilitate mission planning and follow-up observations of afterglows with interesting X-ray spectra.

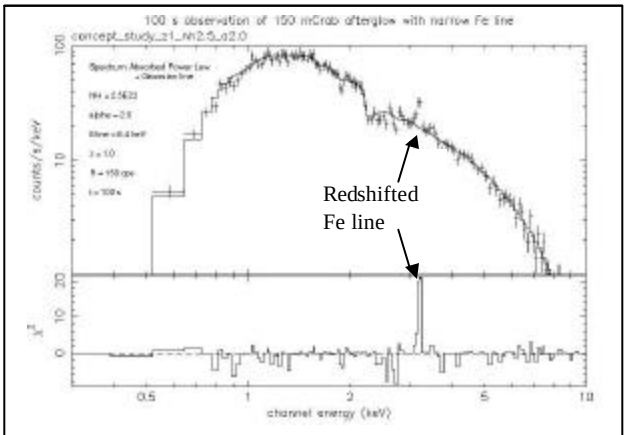

Fig. 7: Simulated spectrum from 100 s *XRT* observation of a 150 mCrab afterglow at z=1.0, assuming a power law spectrum plus a redshifted Gaussian Fe line (E_{rest}=6.4 keV).

The *XRT* readout modes are designed to provide spectroscopic information for sources up to twice as bright as the Crab nebula (~$6x10^{-8}$ ergs/cm^2/s). Sources brighter than this will be piled up even in the fastest readout mode. For more information on XRT readout modes, please see the following paper[11].

Light Curves: The *XRT* is required to provide accurate photometry and light curves with at least 10 ms time resolution. Two timing modes have been implemented, based on the timing modes used on *JET-X* and *Chandra/ACIS*.
Photodiode mode provides the best time resolution (0.14 ms), but integrates the count rate over the entire CCD and therefore provides no spatial information.
Windowed timing mode provides about 2 ms time resolution with 1-D spatial resolution within a window 8 arcminutes wide.

Photometric accuracy will be good to 10% for source fluxes ranging from our sensitivity limit of $2x10^{-14}$ ergs/cm^2/s (in 10^4 s) to roughly $8x10^{-7}$ ergs/cm^2/s. Figure 8 shows a light curve from Panter calibration data with the incident flux ranging over five orders of magnitude. *XRT* light curves will begin when the GRB enters the *XRT* field of view.

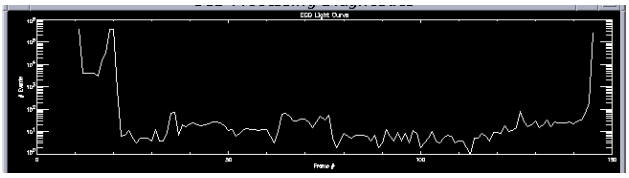

Fig. 8: *XRT* light curve during Panter tests, with incident flux ranging over 5 orders of magnitude.

4 INSTRUMENT DESCRIPTION

4.1 STRUCTURE

The layout of the *XRT* is shown in Figures 2 and 3. The XRT structure is designed around an aluminum Optical Bench Interface Flange (OBIF), with a forward telescope tube supporting the star trackers and the *XRT* Door Module and an aft telescope tube supporting the Focal Plane Camera Assembly. The total mass of the *XRT*, excluding the heat pipe/radiator system, is 198.1 kg.

Optical Bench Interface Flange: The Optical Bench Interface Flange (OBIF; see Figure 11) is the primary structural element of the *XRT* and is responsible for supporting the forward and aft telescope tubes, the Mirror Module, the Electron Deflector, and the TAM optics and camera. It also provides the interface to the *Swift* Optical Bench.

Telescope Tube: This 508 mm diameter graphite fiber/cyanate ester tube, manufactured by ATK, is composed of two sections. The carbon fiber layup is designed to minimize the longitudinal coefficient of thermal expansion so that temperature gradients will not adversely affect the alignment or focus. The composite tube is lined internally with an aluminum foil vapor barrier to guard against outgassing of water vapor or epoxy contaminants into the telescope interior. The rear tube supports the Focal Plane Camera Assembly, and incorporates internal optical baffles. The forward telescope tube section encloses the mirrors and supports the door assembly and the star trackers.

Door: The telescope tube is sealed at the forward end by a single-shot door assembly built by Starsys. The door is designed to protect the X-ray mirrors from contamination during ground operations and launch. This door will be opened about two weeks after launch, which gives the spacecraft time to outgas before exposing the mirrors.

4.2 OPTICS

Overall description: The *XRT* mirror assembly consists of the X-ray mirror module (Figure 9), a thermal baffle mounted in front of the mirrors, a mirror collar that mates to the *XRT* optical bench interface flange, and an electron deflector that mounts behind the mirrors.

***XRT* Mirrors:** The *XRT* uses the FM3 mirror set built and calibrated for the *JET-X* program[1,8] (Figure 9). The mirror module has 12 concentric gold-coated electroformed Ni

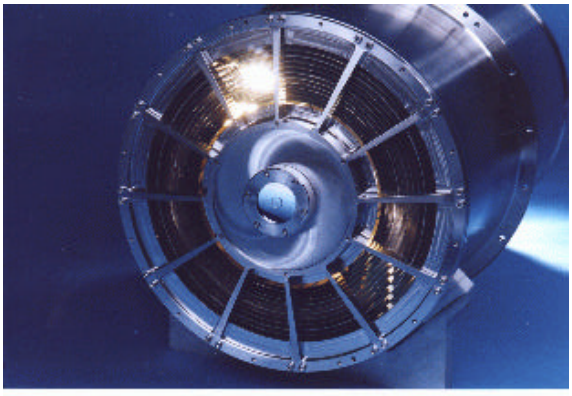

Fig. 9: The *Swift XRT* mirror module.

shells with focal length 3500 mm. The shells are 600 mm long with diameters ranging from 191 to 300 mm. The effective area and point spread function of the mirrors have been measured for a variety of energies and off-axis angles, and were recalibrated at the Panter facility in July 2000. Calibration images (for two sources displaced by 20 arcseconds) and the measured angular resolution of the

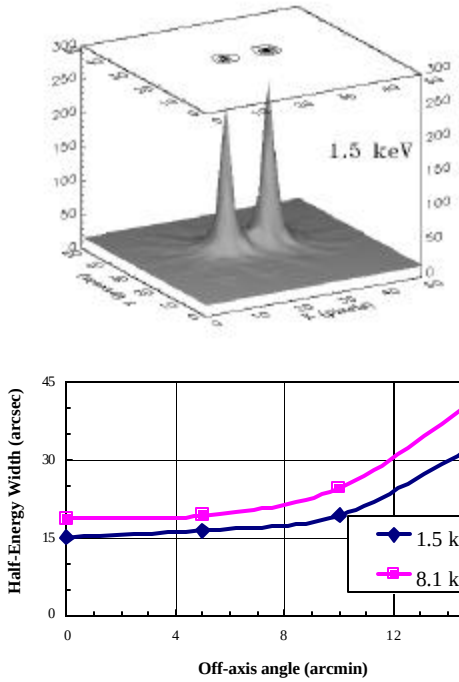

Fig. 10: Measured performance of *XRT* mirrors at 1.5 keV and 8.1 keV. Inset shows an image of two point sources displaced by 20 arcseconds.

mirrors are shown in Figure 10 for two energies, 1.5 keV and 8.1 keV. As noted above, the detector is slightly defocused in the flight instrument in order to optimize the angular resolution over the field of view. Results of the end-to-end calibration of the *XRT* effective area and Point Spread Function are given in accompanying papers in this volume[9, 13].

Thermal Baffle: A thermal baffle in front of the mirror prevents temperature gradients in the mirror that can distort the figure and degrade its Point Spread Function (PSF). Its temperature is actively controlled by heaters, which balance the heat lost to space by the mirrors. The mirror baffle performed well during instrument thermal vacuum tests at NASA/Goddard Space Flight Center, where the flight mirrors were replaced with an identical mirror set with thermal instrumentation.

Electron Deflection Magnets: The electron flux in our 600 km, 22° orbit will produce a variable detector background. An electron deflector, consisting of a system of 12 rare earth magnets, is installed on the OBIF (Figure 11) just behind the rear face of the mirror module to prevent electrons that pass through the mirror from reaching the detector. The design is scaled down from the *XMM* electron deflectors, and has a cutoff energy of ~22 keV with near-zero dipole moment.

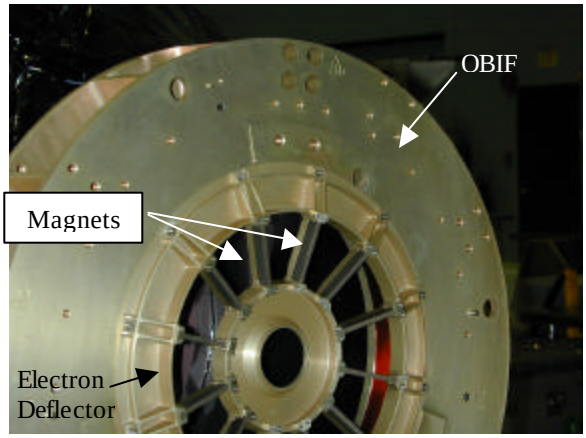

Fig. 11: XRT Electron Deflector, mounted on the Optical Bench Interface Flange (OBIF).

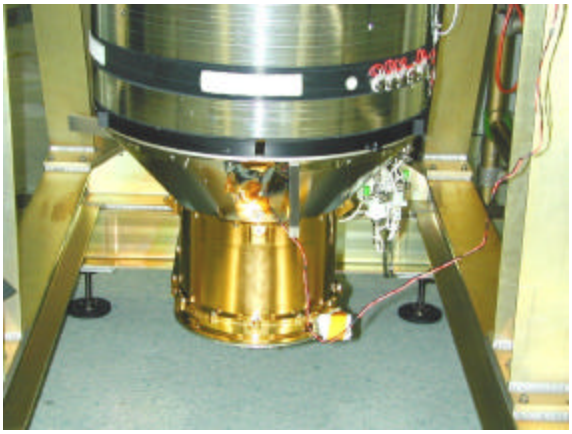

Fig. 13: Focal Plane Camera Assembly (gold), mounted on the XRT rear telescope tube (silver).

4.3 FOCAL PLANE CAMERA ASSEMBLY (FPCA)

The FPCA (Figures 12, 13) provides a vacuum enclosure for the CCD and optical blocking filter during ground operations and launch, shielding for the CCD against trapped protons and cosmic rays, and cooling for the detector. The cryostat has a single-shot door mechanism utilizing redundant Starsys actuators.

The cryostat is attached to a conical interface section that mounts onto the rear tube, supports the cryostat door control hardware and radiator interface, and incorporates a baffled venting system. The vent port allows the telescope internal volume to vent during vacuum testing and launch, while preventing scattered light from entering the CCD enclosure.

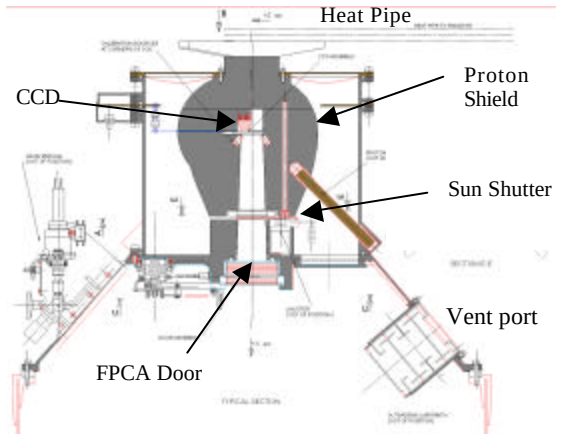

Fig. 12: FPCA cross-section. The entire proton shield is cooled to a temperature of –45 C to –85 C by a radiator/heat pipe system. A TEC integrated into the CCD flight package maintains the CCD temperature at -100 C, using a closed-loop cooling control system. The FPCA also houses the XRT baffled vent.

A novel feature of the FPCA is the sun shutter, which is a safety mechanism designed to autonomously protect the CCD and filter from accidental solar illumination in the event of an attitude control failure. The sun shutter is powered by a Ga-As array mounted at the top of the mirror baffle, which provides power to the sun shutter electronics if the spacecraft slews to within 30 degrees of the Sun, even if the instrument is turned off. If the XRT is pointed closer than 10 degrees to the Sun, the sun shutter is automatically actuated. It can also be opened or closed manually.

The FPCA also houses two sets of calibration sources. An image collected during thermal vacuum testing in July 2002 is shown in Figure 14. The central circular region shows the circular field of view (FOV) of the instrument (defined by the circular optical blocking filter housing,

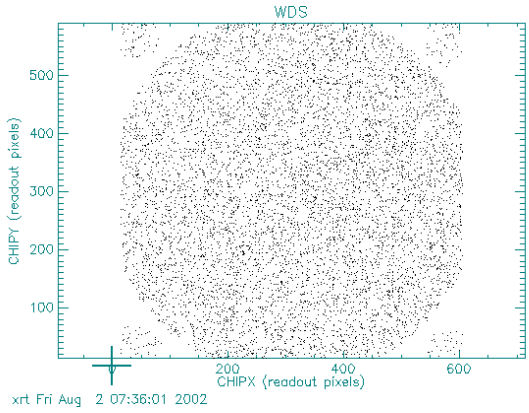

Fig. 14: XRT image of on-board calibration sources. The large central circle shows the instrument field of view illuminated by a calibration source mounted on the inside of the camera door. The four circles of X-rays in the CCD corners are from sources that illuminate the CCD corners continuously during flight.

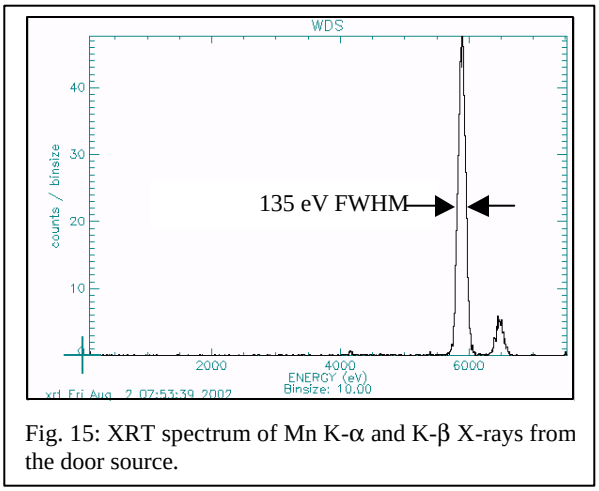

Fig. 15: XRT spectrum of Mn K-α and K-β X-rays from the door source.

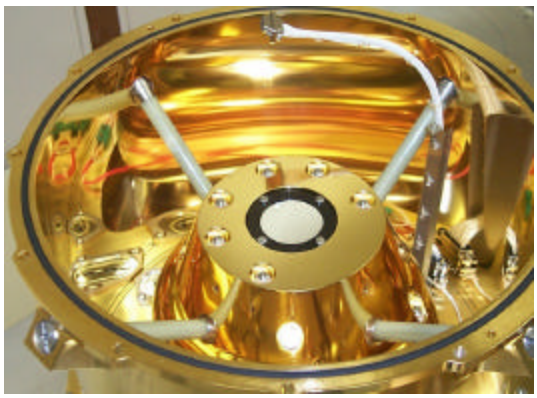

Fig. 16: Interior of the FPCA, showing the lower half of the camera. The circular UV/optical blocking filter is mounted at the top of the lower proton shield, which is mechanically supported by four fiberglass struts. The black ring around the filter is the filter frame, which defines the instrument field of view. The sun shutter assembly mounts immediately above the filter.

but slightly truncated by the edges of the CCD), which is illuminated by Mn K-α and K-β X-rays at 5.9 and 6.4 keV produced by a ^{55}Fe source located on the camera door. The spectrum of these events is shown in Figure 15. During flight this source is moved out of the FOV when the camera door is opened, and this portion of the CCD views the sky. The four circular clusters of X-ray events in the corners of the detector are the in-flight calibration sources, which permit us to measure resolution, gain, and charge transfer efficiency throughout the mission.

Optical Blocking Filter: A thin Luxel filter is installed in front of the CCD to block optical light. The filter is similar to those used on the *Chandra/ACIS* and *XMM/EPIC* instruments. It consists of a single fixed polyimide film 1840Å thick, coated on one side with 488Å of aluminum. The optical transmission of the filter is about 2.5x10^{-3}. The filter can be seen in the center of Figure 16, which shows the interior of the FPCA.

4.4 *XRT* DETECTORS

CCD Architecture: The CCD-22 detector, designed for the *EPIC* MOS cameras on *XMM-Newton* by E2V (formerly known as EEV), is a three-phase frame-transfer device, which utilizes high resistivity silicon and an open-electrode structure[3] to achieve a useful bandpass of 0.2 to 10 keV[4]. A simplified schematic is given in Figure 17. It has an imaging area of ~2.4 x 2.4 cm. The image section of each CCD is a 600 x 602 array of 40μm x 40μm pixels, each pixel corresponding to 2.36 arcseconds in the *Swift* focal plane. The storage region is a 600 x 602 pixel array of 39 x 12 μm pitch. The readout register is split into two sections, and may be read out using either output node, or

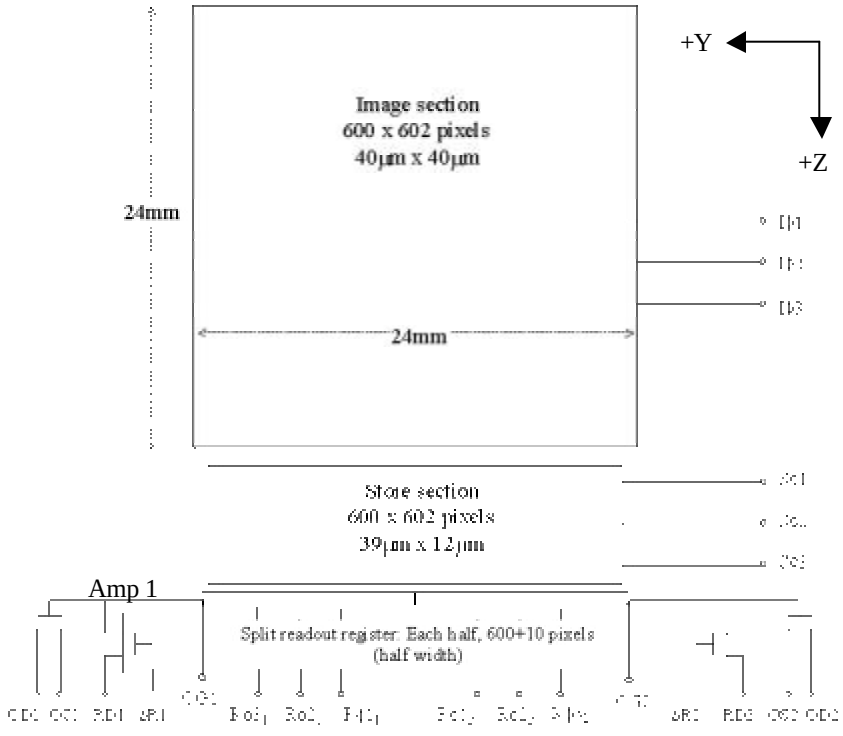

Fig. 17: CCD22 simplified schematic. Instrument axes are indicated.

may be split and read out using both nodes simultaneously; the *XRT* waveforms do not utilize the split readout capability. The CCD may also be operated in timing mode or window mode, which allow faster readout of fewer pixels so that bright sources may be observed without saturation.

Energy Resolution: The energy resolution of the CCDs is shown in Figure 18, in which the dotted line is the ideal (Fano-limited) resolution, the solid line is the predicted resolution for an *EPIC* MOS CCD and the points are measurements from a typical flight device. Below ~ 500 eV the effects of charge trapping and loss to surface states become significant.

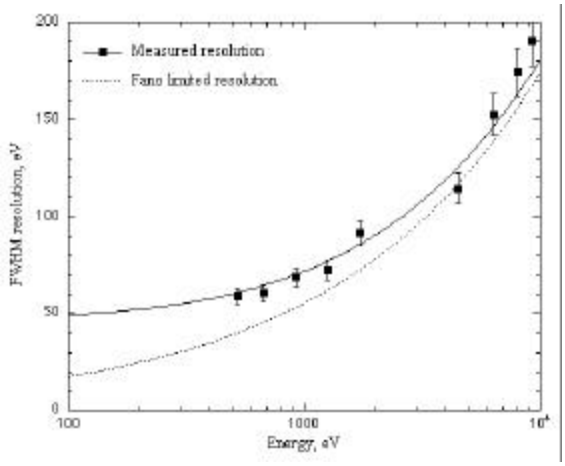

Fig. 18: CCD-22 energy resolution above 500 eV.

QE: The QE of an X-ray CCD is determined at low energies by the gate structure and at high energies by the depletion depth. A special "open-gate" electrode structure gives the CCD-22 excellent low energy quantum efficiency, while high resistivity silicon provides a depletion depth of 30 to 35μm to give good QE at high energies. Quantum efficiency measurements of these detectors have been made at the University of Leicester and at the Orsay Synchrotron. These measurements have been incorporated into Monte-Carlo and analytical models developed for *XMM/EPIC* to simulate the quantum efficiency and spectral response of the CCDs. These models have been used to construct *XRT* response matrices as described in an accompanying paper[14].

Radiation Hardness: CCDs are susceptible to both ionizing and non-ionizing radiation damage, but the primary area of concern for an X-ray photon-counting CCD spectrometer in low Earth orbit is displacement damage caused by proton irradiation, which results in the creation of electron traps in the silicon lattice. These traps degrade the charge transfer efficiency of the device over time and directly degrade its energy resolution. We note that the ability of the CCD to measure accurate source positions and lightcurves is unaffected by this proton damage until doses far in excess of the total *Swift* mission dose are reached.

We have performed a radiation study for the *XRT* in the baseline *Swift* orbit of 600 km altitude and 22° inclination. This study indicates that the equivalent 10 MeV proton flux seen by the *XRT* detectors is 3.4×10^8 protons/cm^2/yr. The expected total dose for the *XRT* in a nominal two-year mission is comparable to the total mission fluence of 5×10^8 protons/cm^2 expected for *XMM*. Considerable analysis and laboratory test data from the *EPIC* program are therefore directly applicable to the *XRT*. Laboratory measurements using CCD-22s irradiated to 2.5×10^8 10 MeV protons/cm^2 have been used to verify that the *XRT* will achieve its end-of-life requirement of 300 eV resolution for 6 keV X-rays.

4.5 THERMAL DESIGN

Cryostat: X-ray CCD detectors must be cooled to between –80 C and –130 C during operation to ensure low dark current and to reduce sensitivity to radiation damage. The *XRT* CCD will be cooled by a Marlow Thermo-Electric Cooler (TEC) to –100 C, with the heat dumped to a radiator sitting at –85 C to –45 C (depending on orbital parameters and spacecraft orientation). Thermal vacuum tests on both the instrument and the Heat Rejection System show that we can easily meet the thermal requirements during flight.

Heat Rejection System (HRS): The HRS design is dictated by the *Swift* orbit and pointing constraints. It consists of dual redundant ethane heat pipes and a 900 cm^2 radiator coated with AZW-LA-II paint. The radiator is carefully configured and integrated with the external spacecraft design to achieve the required low temperature of –85 to –45 C in low Earth orbit.

Telescope thermal design: The *XRT* uses both passive design features and active thermal control to achieve the high degree of dimensional stability required for arcsecond alignment tolerances. Operational heaters on the telescope tube are thermostatically controlled in 36 independent zones (arranged in 9 bands, each with four quadrants) to maintain a constant longitudinal thermal gradient and less than 2 C azimuthal thermal gradient on the telescope tube, and are placed to eliminate longitudinal and azimuthal temperature gradients that could distort the tube. Figure 19 shows a close-up of two of these heater elements, and Figure 20 shows the location of all 9 operational heater bands. Within each quadrant an RTD sensor measures the temperature of that quadrant. These

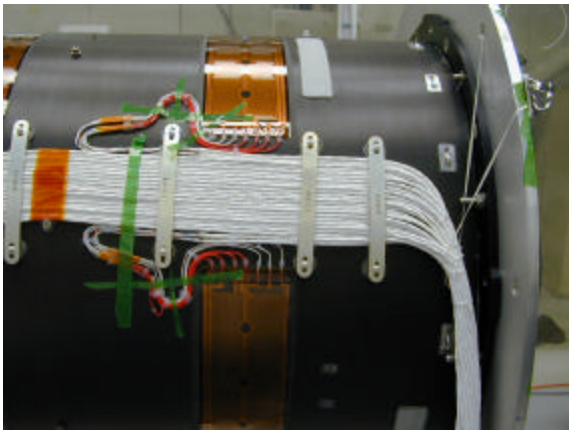

Fig. 19: Aft tube heater detail, showing connection of the heater harness to two heater elements.

data are monitored by our housekeeping circuits once per second. Every 30 seconds the XRT software compares each quadrant's temperature to an adjustable setpoint for that quadrant and turns the corresponding heater on or off accordingly. The setpoint and deadband (hysteresis) of each quadrant is independently adjustable. This system performed well during thermal balance tests.

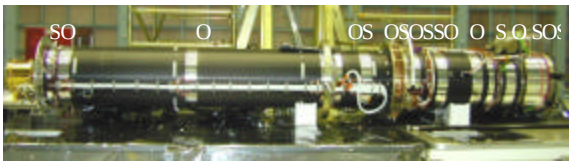

Fig. 20: Side view of the assembled XRT. The silver bands are the operational and survival heater elements. Operational heaters are indicated by an "O", and survival heaters are indicated by an "S".

Survival heaters are designed to prevent damage to the instrument when the instrument power is off. Survival heaters are located on the telescope tube at bonded joints to the metal reinforcing rings and flanges, which have much higher expansion coefficients than the composite tube, and on the electronics box.

Mirror thermal design: The mirror module must be maintained at 20 C +/- 0.5 C with a delta of less than 1 C from front to back in order to prevent degradation of the mirror PSF. The mirrors are not heated directly; instead, an actively controlled thermal baffle in front of the mirrors replaces the heat radiated to space by the mirrors. The heaters on the mirror baffle are critical to the proper figure and performance of the telescope mirrors. Thermal control is provided by two control heater pairs (one each on the inner and outer mirror baffles) regulated by the flight software to adjustable setpoints in the same way that the operational tube heaters are controlled. During thermal balance tests the mirror baffles successfully maintained the thermal gradient along the mirrors at a few tenths of a degree Celsius.

4.6 TELESCOPE ALIGNMENT MONITOR (TAM)

Although we expect the composite tube/heater thermal system to provide a stable platform, the *XRT* will be operating in an unusually dynamic thermal environment. As an additional measure to correct for any thermal variations in the instrument alignment, the *XRT* has an internal Telescope Alignment Monitor (TAM) designed to actively measure any remaining alignment errors between the *XRT* boresight and the star trackers.

The TAM (Figure 21) uses two redundant LEDs mounted on the FPCA, which are observed by a small radiation-hard programmable CMOS active pixel sensor camera developed for space applications by SIRA Electro-Optics. The TAM camera and optics block are mounted on the optical bench interface flange (OBIF), which is the hard mount point for the forward and aft telescope tubes and the mirror module, and which is mounted in turn to the *Swift* optical bench. The TAM camera monitors two light paths: the direct path from the FPCA LED, and a secondary path that includes a reflection from a mirror mounted to the star tracker platform. The direct path monitors lateral motion of the FPCA relative to the OBIF, which defines (to first order) the XRT boresight. The secondary path monitors changes in the tilt of the star trackers relative to the OBIF, and is sensitive to deviations in the star tracker boresight. These two paths produce two images of the LED, which are independently monitored and telemetered.

The TAM window measurements will be made every 1-5 minutes during the mission. The TAM centroids will be calculated and will be used on-board to calculate GRB positions to be telemetered to the GCN. They will also be telemetered in the science telemetry stream for use by ground processing software to construct accurate sky maps for both the *XRT* and the *UVOT*.

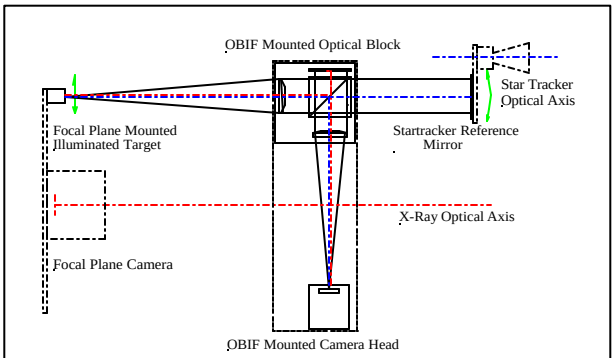

Fig. 21: Telescope Alignment Monitor optical design.

We have performed several tests to verify the accuracy and utility of the TAM data. Figure 22 shows the displacement of TAM centroid positions in the primary window as the telescope tube heaters were used to heat the rear tube anisotropically to force it to bend slightly. Movement of the TAM image by less than 0.05 TAM pixels (one vertical division), corresponding to movement of the *XRT* boresight by less than 0.5 arcseconds, is easily measurable.

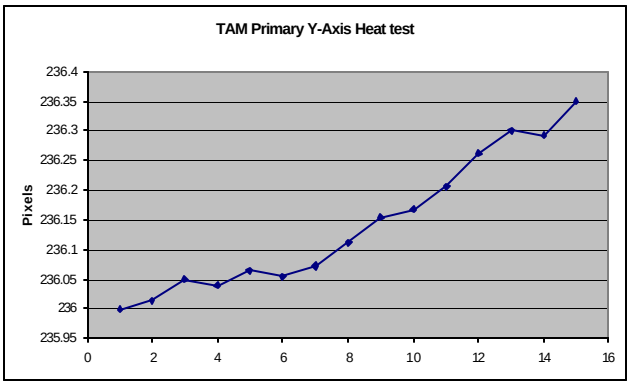

Fig. 22: TAM measurement of tube bending due to anisotropic heating of rear telescope tube.

4.7 ELECTRONICS DESIGN

The overall electronics design is shown in the block diagram in Figure 23. The electronics design has been discussed in some detail previously[15]. Here we briefly mention some of the key subcomponents. Analog and digital electronics are located in separate portions of a single physical box, with a shield layer between the analog and digital portions.

4.7.1 Digital Electronics

The *XRT* digital electronics architecture has four main functional blocks: the Instrument Control Processor (ICP; a Mars98 RAD6000 board); the Clock Sequencer board, which controls the CCD readout waveforms; the Relay board, which controls power to operational tube and mirror baffle heaters; and the Communications Module, which includes the S/C interface and the clock synchronization circuitry. These boards reside on a VME bus.

The spacecraft interface board contains the *XRT* clock and the circuitry necessary to synchronize the *XRT* clock to the spacecraft clock. The spacecraft clock value is sent to the *XRT* once per second, along with a clock pulse that allows us to synchronize the time. The *XRT* uses this clock pulse to latch the spacecraft clock time into the *XRT* Mission Elapsed Timer register once per second to ensure synchronization with the spacecraft clock. Ground-based software converts from spacecraft time to Universal Time.

The camera control/clock sequencer board controls the CCD camera and data interface. The Clock Sequencer is a DSP-based state generator utilizing a rad-hard Analog Devices AD-21020, and is based on our laboratory camera design[16]. The logic levels produced by the Clock Sequencer drive the Clock Driver board, which in turn generates the analog CCD clocking voltages.

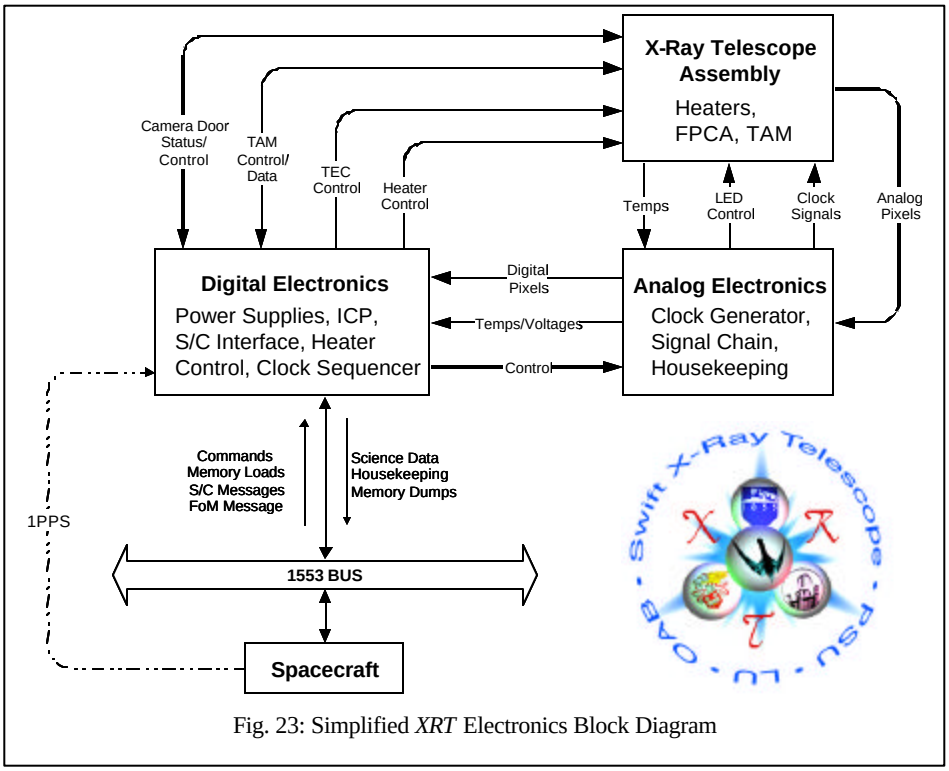

Fig. 23: Simplified *XRT* Electronics Block Diagram

4.7.2 Analog Electronics

The analog electronics are housed in a separate chamber within the electronics box in order to isolate the sensitive analog electronics from the noisy digital signals. The analog electronics consist of CCD drivers, dual signal chains, and analog housekeeping. The dual signal chains extract the CCD signal packets from the detector video signal, using a correlated double sampler. The CCD drivers convert the digital CCD clock pulses to analog clock voltages, with voltage levels and bias levels set by DACs so that they can be changed by ground command if needed to offset any flat band shifts during the mission.

The preamps are based on the *XMM/EPIC* design. They are housed inside the CCD camera to minimize noise pickup. The camera headboard contains 2 preamplifiers, which are AC coupled to the two output nodes of the CCD. In order to achieve the necessary slew rates and noise performance PMI OP37 preamps are used in non-inverting configuration with a gain of around X16. A noise figure of better than 5 e^- rms has been achieved at system level with this front-end.

4.7.3 TEC Power Supply

The Peltier cooler (TEC) is operated by a variable voltage power supply designed by R. Green of PSU. The output voltage is controlled by the flight software. In "manual mode" the software controls the power supply output voltage to a set value, while in "automatic mode" it controls the CCD temperature by adjusting the TEC voltage as needed to maintain a constant temperature. The TEC power supply and control software achieve temperature stability better than ±0.5 C in auto mode, as shown in Figure 24. The power supply can also be used to heat the CCD by reversing the output polarity under software control.

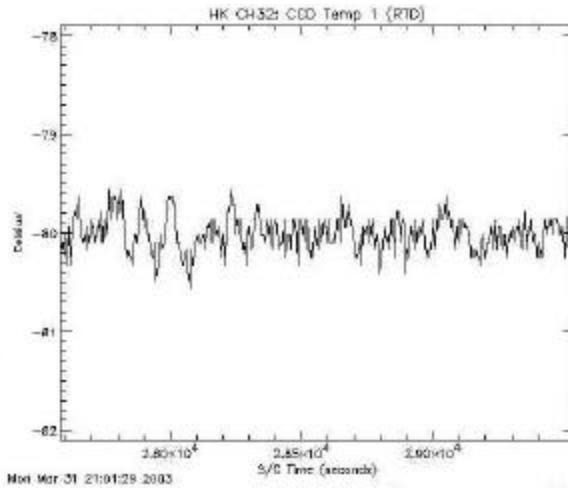

Fig. 24: CCD Temperature stability under closed-loop control of TEC Power Supply and control software. In this laboratory test the camera temperature was –35C and the CCD set point was –80C.

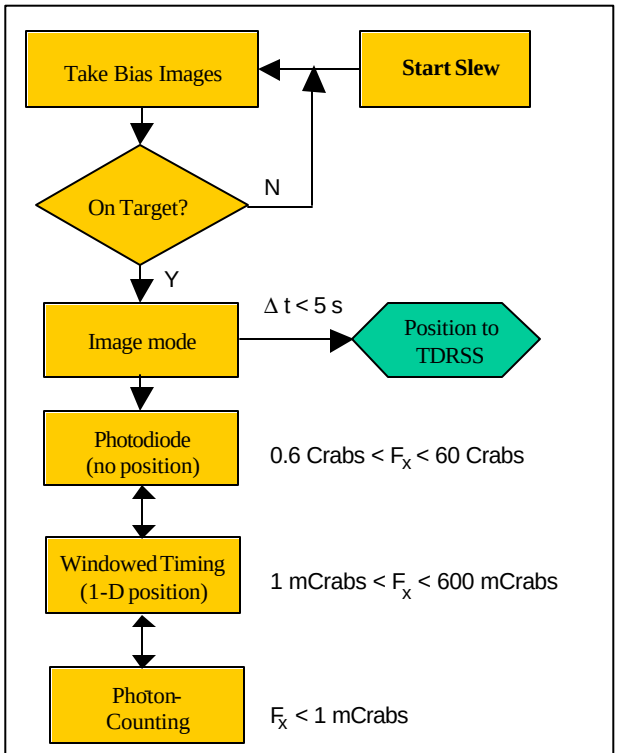

Fig. 25: Swift XRT Automated Observing Sequence for a new GRB. Observation begins with a slew to the target. During the slew we collect bias information for all readout modes. At the end of the slew we take an image which is centroided to provide the burst location. We then switch into timing modes designed to maximize science return without saturating the detector. For low count rates we switch to a more standard X-ray CCD readout mode which records the position, grade, and energy of each photon.

4.8 AUTOMATED OPERATIONS

Because the *Swift* spacecraft must respond rapidly to new targets, the spacecraft instruments must be able to operate autonomously. This poses interesting new problems for the instrument design. Over the course of a typical GRB observation, the burst/afterglow flux will decrease by many orders of magnitude, and we must be able to observe over this wide dynamic range without detector saturation at early times when the burst and afterglow are bright, while preserving as much information about the incident photons as possible. The *XRT* is designed for completely autonomous operation, switching between different readout modes according to the instantaneous count rate in each CCD frame, as shown in Figure 25. The autonomous operation of the *XRT* and its readout

modes are described in more detail in the following paper[11]. We briefly describe the readout modes here:

1. Imaging mode: the CCD is operated like an optical CCD, collecting the accumulated charge from the target and reading it out *without* any X-ray event recognition. For a typical GRB, this image will be highly piled-up and will therefore produce no spectroscopic data, but it will produce an accurate position and a good flux estimate. Image mode is operated with low gain to allow observations up to the full well capacity of the CCD (in normal gain, we are limited by the ADC range rather than the full-well). It uses either 0.1 or 2.5 second exposures, depending on the source flux. Imaging mode can be used to determine on-board centroids for source fluxes between 25 mCrabs and 37 Crabs. The following data products are produced: the GRB centroid position and X-ray flux estimate (telemetered through TDRSS and distributed immediately to the community through the Gamma-ray burst Coordinate Network (GCN[17]); a postage-stamp image (2'×2'), also telemetered via TDRSS and distributed through the GCN; and a compressed image (pixels above a threshold) in our normal science telemetry stream. The X-ray flux estimate assumes a Crab-like spectrum.

2. Photodiode mode: a fast timing mode designed to produce accurate timing information for extremely bright sources. This mode alternately clocks the parallel and serial clocks by one pixel each. Charge is accumulated in the serial register during each parallel transfer, with the result that each digitized pixel contains charge integrated from the entire field of view (although not simultaneously). For the GRB case, where we expect the image to be dominated by a single bright source, photodiode mode produces a high-speed light curve with time resolution of about 0.14 ms. This mode is useful for incident fluxes below 60 Crabs, and has manageable pileup for fluxes below 2 Crabs. Data products in photodiode mode are FITS binary table files with the time, energy, and grade (or pattern) of each recorded event (unless the data are too piled-up to identify individual photon events).

3. Windowed Timing mode: restricted to a 200 column window covering the central 8 arcminutes of the FOV. Imaging information is preserved in one dimension (in Right Ascension for zero degrees spacecraft roll). Pixels are binned by 10x along columns. This mode has 2.2 ms time resolution for a 200 pixel window. It is useful for fluxes below 5000 mCrabs, and has minimal pileup below 1000 mCrabs. Data products are FITS binary table files with the 1-D position, arrival time, energy, and pattern of each event.

4. Photon-counting mode: retains full imaging and spectroscopic resolution, but time resolution is only 2.5 seconds. It is useful below 1 mCrab. Data products are FITS binary table files with the 2-D position, arrival time, energy, 3×3 pixel "neighborhood" centered on the event, and the grade (or pattern) of each event. Grades are recorded using a scheme similar to the *XMM-EPIC MOS* pattern library.

In order to cope with the rapidly changing source flux of GRBs, the *XRT* will automatically determine the optimum readout mode for the current source intensity and adjust its readout and processing modes accordingly. The algorithm we have designed, shown in simplified form in Figure 25 and in more detail in the following paper[11], will ensure the maximum science return for sources ranging over more than 7 orders of magnitude in flux. This algorithm was successfully tested at the Panter X-ray facility using a variable source flux designed to mimic the behavior we expect from real GRBs (Figure 8).

4.9 *XRT* SOFTWARE

4.9.1 Flight Software

There are two main pieces of flight software:

- The Instrument Control Processor (ICP; this is the RAD6000 CPU) software is responsible for instrument control, data collection and processing, and spacecraft interfacing. The ICP software is written in C and runs under the VxWorks operating system. On boot-up, the code performs self-tests and enters Manual State with the CCD in Null mode (clocks running but no digitization of the data). Manual state is used for engineering tests, calibration, or instrument configuration. Once commanded into Auto State, the software automatically collects and processes data as described in more detail in the following paper[11]. Background processes ingest data from the TAM and transmit telemetry data to the spacecraft.
- The Clock Sequencer code is generated by an IDL program that uses a graphical user interface to produce 21020 DSP assembler code. It supports a number of readout modes, including standard readouts in different CCD modes, plus diagnostic modes that facilitate checkout of the camera during ground tests and on orbit.

Flight software for both the ICP and Clock Sequencer is tested on engineering units before installation on the flight hardware.

4.9.2 Processing and Analysis Software

The Swift Data Center (SDC) at NASA/GSFC is responsible for the Level 0 software, which produces time-ordered telemetry data, and Level 1 software, which produces standard format FITS event files. Level 2 software, called *XRTDAS*, consists of a set of FTOOLS written by the ASI Science Data Center (ASDC), and will support both pipeline and interactive data analysis. *XRTDAS* will be publicly available from the HEASARC at NASA/GSFC prior to the launch of *Swift*.

5 OPERATIONS

With the exception of occasional manual calibration observations, the operation of the XRT is completely autonomous and is driven by the response of the observatory to its on-board observation timeline and to newly discovered GRBs. The *Swift* Mission Operations Center (MOC) will load pre-planned target (PPT) timelines onto the observatory on a daily basis or as needed. New GRBs trigger Automated Targets (ATs), which are generated on-board by the BAT instrument. A software process called the Figure of Merit process controls the observing timeline and arbitrates between PPTs and ATs according to their assigned observing priorities.

Because the *Swift* observatory is in low Earth orbit, and because the two Narrow-Field Instruments (XRT and UVOT) cannot be pointed closer than 30 degrees to the Earth's limb, there is no "Continuous Viewing Zone" for *Swift*, and all observations will be broken up by observing constraint violations that require the spacecraft to slew to a new target. This results in observations of any given target that are broken into segments of (typically) 20-30 minutes duration, which we refer to as "snapshots", with other objects intervening. This is illustrated graphically in Figure 26. Snapshots are grouped together into "observation segments" that cover 1-2 days.

Figure 27 provides a graphical illustration of a typical "day in the life" of the *XRT*. This shows schematically how a newly discovered GRB (an Automated Target, or AT) interrupts a previously scheduled series of observations (Pre-Planned Targets). Figure 28 shows in more detail the sequence of events at the beginning of an AT and the data products generated in both the TDRSS telemetry channel and the normal science telemetry channel.

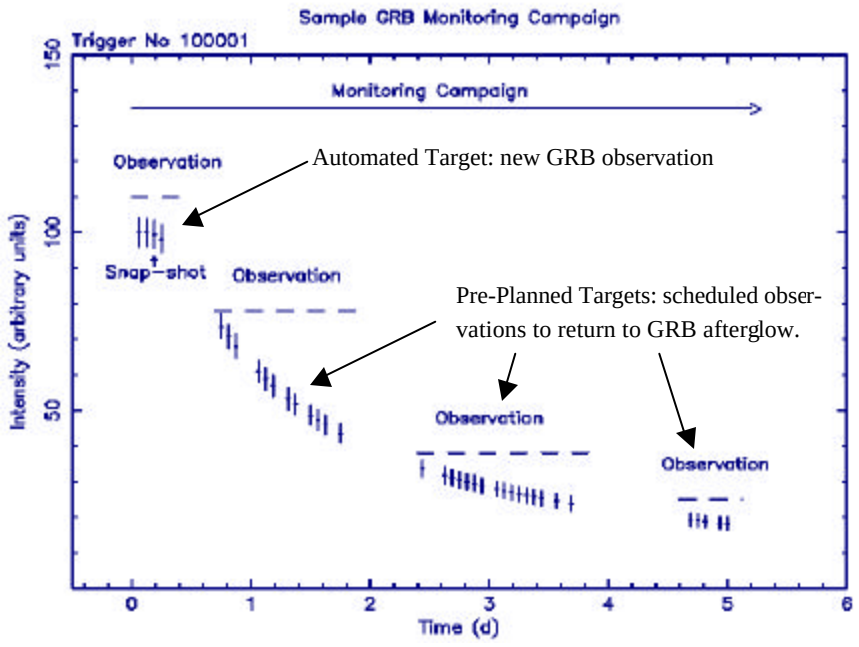

Fig 26: Typical *Swift* observing program for a new GRB. The observing program is broken into several "observation segments", each lasting 1-2 days, which are in turn broken into "snapshots" of typical duration 20-30 minutes. The first observation segment is scheduled automatically on-board and lasts 20,000 s (on-target). Subsequent observation segments are pre-planned on the ground as updates to the mission timeline. (Figure courtesy of L. Angelini of NASA/GSFC.)

6 ALIGNMENT AND CALIBRATION

6.1 ALIGNMENT

The telescope optical pointing direction or boresight has been established by using a micro-alignment telescope (MAT) mounted on a special alignment jig to accurately measure the line from the center of the CCD through the center of the mirror module. The measured boresight has been transferred to the external alignment reference cube, using optical transfer flats and an additional autocollimator.

After mounting the flight mirrors, co-alignment of the external alignment reference cube was checked against the mirror optical reference flat. No additional shimming was found to be necessary.

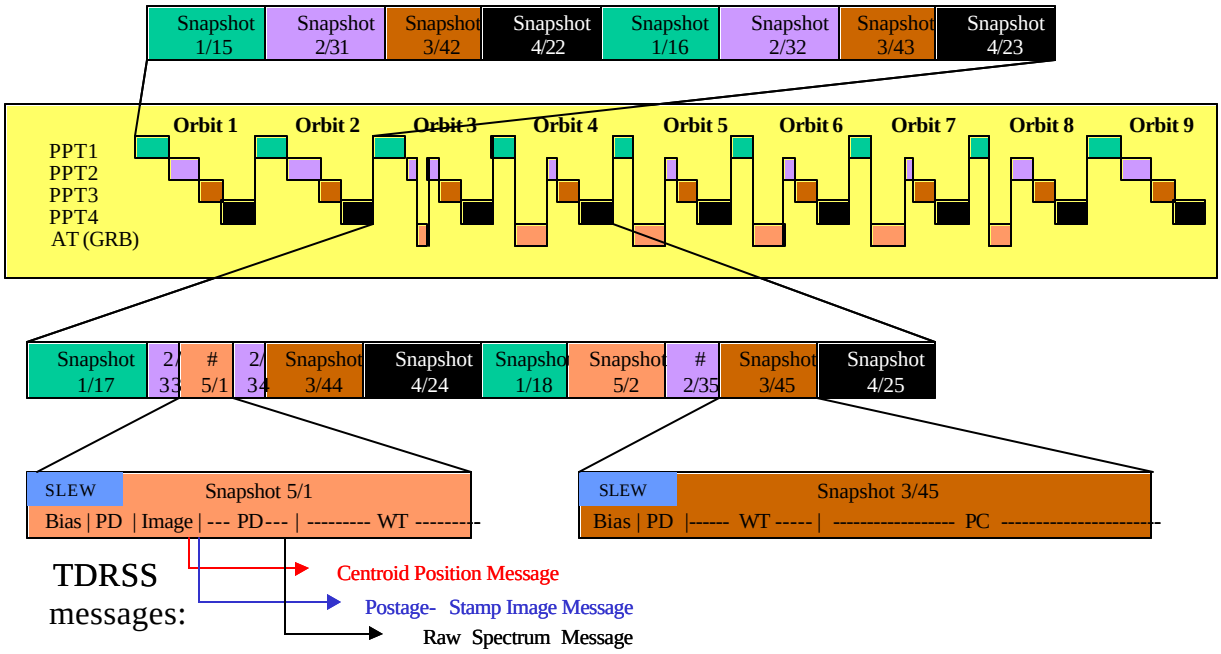

Fig. 27: Pictorial diagram of a typical "day in the life" of *XRT* observations covering 9 orbits. The middle box (yellow) shows a timeline for a sequence of snapshots of 5 different targets, four Pre-Planned Targets (PPTs) loaded into the on-board flight timeline, and one Automated Target (AT) representing a newly discovered GRB. Targets are color-coded for clarity. The top bar shows an expanded view of the first two orbits. Snapshots are identified by a target number and a snapshot number (target/snapshot). These PPTs would typically represent follow-up observations of GRBs discovered over the previous week. In Orbit 3 a new GRB is discovered by the BAT, and the FOM task assigns it a target number of 5 and schedules an immediate observation, interrupting the previously-scheduled snapshot 34 for target #2. The automated observation of target #5 continues until it is interrupted by an observing constraint, at which time the FOM resumes the interrupted observation of target #2 with snapshot #34. On Orbit 4, target #5 is observed as soon as it becomes visible, and preempts time from both target #1 and target #2. The bottom bar shows the sequence of *XRT* events for an AT (target #5) and a PPT (target #3). For the AT, the *XRT* updates its bias row and bias map during the slew and then switches into Photodiode (PD) mode. As soon as the slew ends, the *XRT* takes an image, centroids the image to determine the source position, and sends this to the ground through TDRSS, along with a postage-stamp image of the source. It then switches back to Photodiode mode until the flux drops low enough for Windowed Timing (WT) mode, at which point it sends a cumulative raw spectrum to the ground through TDRSS. The sequence of events for a PPT is similar, except that no Image Mode data are collected and no TDRSS messages are generated.

Following alignment, the *XRT* master alignment cube defines the *XRT* instrument axes, with the X-axis parallel to the *XRT* boresight (+X towards the target), the Y-axis parallel to the CCD serial register, and +Z in the parallel readout direction (Figure 16).

6.2 CALIBRATION

The *XRT* detectors and optical blocking filter were calibrated at the University of Leicester and the mirrors were calibrated at the Panter facility. End-to-end testing and calibration of the fully assembled instrument was performed in September 2002 at the Panter X-ray Calibration Facility in Munich. This end-to-end calibration verified the instrument point spread function, effective area, and focus. Results of these calibrations are presented in several papers in this volume[9, 13, 14] and are incorporated in the *XRT* response matrices.

CCD Selection and Calibration: *Swift/XRT* CCDs were tested, characterized, and calibrated in the calibration facility at the University of Leicester. This facility uses Kevex sources and fluorescent targets to generate X-ray line emissions from Carbon Kα (277 eV) to Arsenic Kα (10532 eV). At energies below approximately 1500 eV, a crystal monochromator is used to isolate the desired emission line. The CCDs are mounted on a liquid nitrogen cold finger, and their temperature may be controlled in the range -40 to -140 C. The X-ray beam flux is monitored with a calibrated lithium drifted silicon detector to measure quantum efficiency.

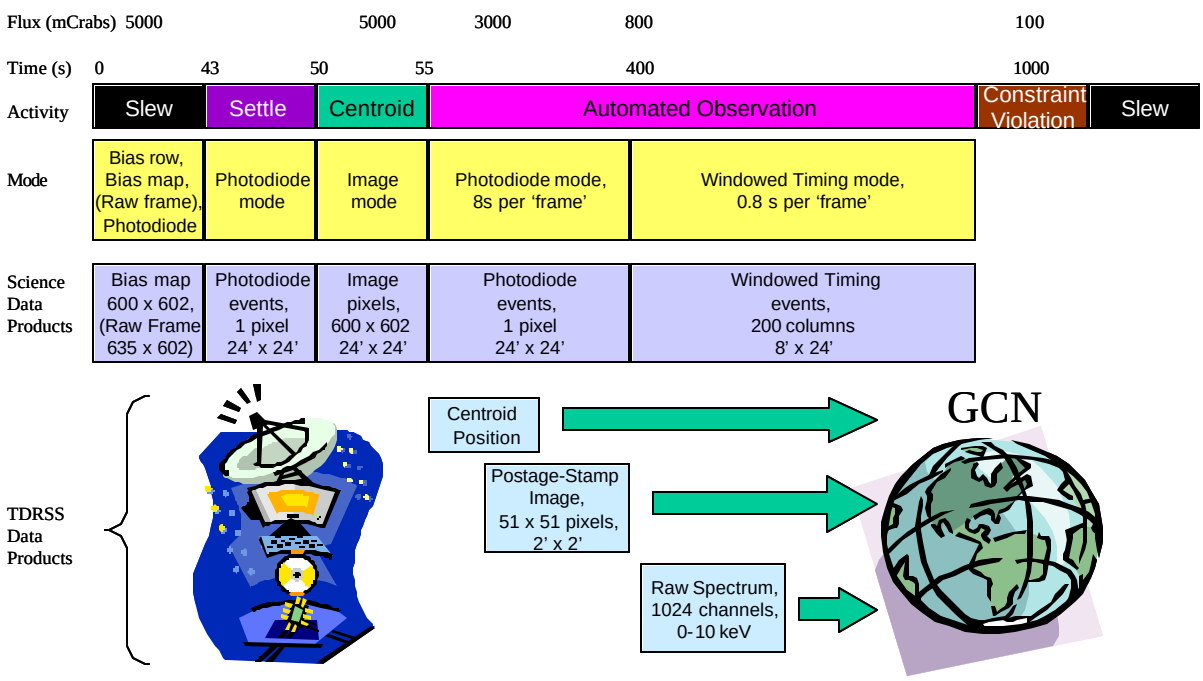

Fig. 28: Timeline of an *XRT* observation of an Automated Target (newly-discovered GRB). The new Snapshot begins when the observatory begins to slew to the new target. A typical slew will take between 20 and 50 s; here we show a slew time of 43 s followed by a worst-case settle time of 7 s. The *XRT* takes up to 5 s to determine the GRB centroid, and then begins the balance of an automated observation. As the flux decays (top line), the *XRT* modes switch accordingly. The Snapshot ends when a constraint violation triggers another slew. *XRT* mode and data products are shown in the center and bottom bars, respectively. TDRSS messages are shown in the bottom graphic. In this case, the Centroid Position message is generated at about 55 s and the Spectrum message is generated at about 400s.

Selection of potential flight devices was based upon cosmetic defects (bright and dark pixels and columns), spectral resolution across the energy band, quantum efficiency and spatial uniformity of the low energy response. One flight and three flight spare devices underwent an initial calibration in the Leicester test facility. X-ray data were acquired over a range of energies, temperatures and flux rates. Approximately a million photons were collected on the flight CCD. The calibration data were used to tune our Monte Carlo CCD model, and response matrices have been generated for all *XRT* readout modes[14].

Mirrors: The flight mirrors were calibrated at the Panter facility in Germany as part of the *JET-X* calibration[1] in 1996 and were stored at the Osservatorio Astronomico di Brera in a dry, inert atmosphere in a hermetically sealed shipping container for the next four years. They were recalibrated in July 2000 at the Panter facility to check for any changes in performance since the original calibration. Analysis of the new calibration data confirms the previous results.

End-to-end Calibration: End-to-end testing of the entire instrument was performed at the Panter X-ray Calibration Facility operated by MPE (Figure 29). This calibration concentrated on four primary measurements:

- Verification of the focus of the telescope.
- Measurement of the on-axis and off-axis PSF of the telescope at several energies to verify that the telescope mounting has not introduced any distortion to the mirrors[9].
- Measurement of the end-to-end effective area at several energies and off-axis angles[13].
- Verification of the operating modes of the instrument, including the automated mode switching[11].

In-Flight Calibration: In-flight calibrations will be performed both during the Performance Verification phase following instrument turn-on, and as an ongoing activity. The PV phase calibration will include the following:

- Calibration of the *XRT* PSF as a function of off-axis angle, and of the boresight alignment relative to the Star Trackers, using bright X-ray

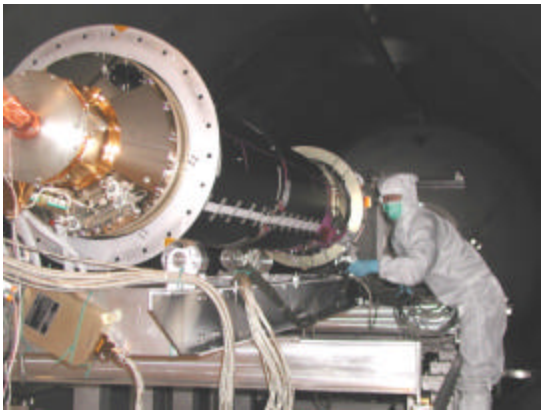

Fig. 29: *XRT* installation into the Panter vacuum chamber, looking towards the X-ray source. The FPCA is in the foreground towards the upper left corner of the photo.

point sources observed in a variety of thermal environments throughout the orbit.

- Calibration of the end-to-end instrument effective area, using the Crab nebula and/or SNR 0540-69 (which have well-known and constant spectra).
- Calibration of the energy response using bright emission line sources such as the Cas A and E0102 supernova remnants.
- Calibration of the timing modes using X-ray pulsars (cross-calibrated to *RXTE*).

These calibration observations will be repeated on a periodic basis (roughly once every six months) to monitor any instrument changes with time.

In addition to calibration with astrophysical sources, the *XRT* will be calibrated on an ongoing basis using four small on-board ^{55}Fe sources that constantly illuminate the corners of the CCD at a low rate. These events (which are spatially distinct from the part of the CCD viewing the sky in all but Photodiode mode) will be tracked as part of our trend analysis to monitor energy resolution, gain, and charge transfer efficiency throughout the mission.

Finally, full CCD images will be sent to the ground on a regular basis to monitor the detector for any changes in hot pixels or other artifacts that could affect our on-board event processing. On-board lists of bad rows, columns, or pixels will be updated based on analysis of these images by the instrument team.

7 ACKNOWLEDGEMENTS

This work is supported at Penn State by NASA contract NAS5-00136; at the University of Leicester by the Particle Physics and Astronomy Research Council on grant number PPA/G/S/00524; and at OAB by funding from AS on grant number I/R/309/02. We gratefully acknowledge the contributions of dozens of members of the *XRT* team at PSU, UL, OAB, GSFC, and our subcontractors, who helped make this instrument possible.

8 REFERENCES

1. O. Citterio *et al*., "Characteristics of the flight model optics for the JET-X telescope onboard the SPECTRUM X-γ satellite", *Proc. SPIE*, **2805**, 56-65, 1996.
2. A. Wells *et al*., "The JET-X Instrument for the USSR Spectrum RG Mission", *Proc. SPIE*, **1546**, 205-220, 1992.
3. A. D. Holland, M. J. L. Turner, A. F. Abbey, P. J. Pool, "MOS CCDs for the EPIC on XMM", *Proc. SPIE*, **2808**, 414-420, 1996.
4. A .D. T. Short, A. Keay, M. J. L. Turner, "Performance of the XMM EPIC MOS CCD Detectors", *Proc. SPIE*, **3445**, 13-27, 1998.
5. J. A Nousek *et al*., *Proc. SPIE*, **5165,** in press, 2004.
6. S. Barthelmy *et al*., *Proc. SPIE*, **5165,** in press, 2004.
7. P. Roming *et al*., "The Swift Ultra-Violet/Optical Telescope", *Proc. SPIE*, **5165,** in press, 2004.
8. A. Wells *et al*., "X-ray Imaging Performance of the Flight Model JET-X Telescope", *Proc. SPIE*, **3114**, 392-403, 1997.
9. A. Moretti *et al*., *Proc. SPIE*, **5165,** in press, 2004.
10. J. Hill *et al*., "An Algorithm for Locating PSF-Like Events and Computing the Centroid in X-ray Images", *Proc. SPIE*, **4851,** 1347-1355, 2003.
11. J. Hill *et al*., "Readout Modes and Automated Operation of the Swift X-ray Telescope", *Proc. SPIE*, **5165,** in press, 2004.
12. De Pasquale *et al.*, "A Comparative Study of the X-ray Afterglow Properties of Optically Bright and Dark Gamma-Ray Bursts", *Astrophys. J.*, **592**, 1018-1024, 2003.
13. G. Tagliaferri *et al*., *Proc. SPIE*, **5165,** in press, 2004.
14. K. Mukerjee *et al*. 2003, *Proc. SPIE*, **5165,** in press, 2004.
15. D. N. Burrows *et al.*, "The Swift X-ray Telescope", *Proc. SPIE*, **4140,** 64-75, 2000.
16. J. Hill *et al.*, "Laboratory X-ray CCD Camera Electronics – a test bed for the Swift X-ray Telescope", *Proc. SPIE*, **4140,** 87-98, 2000.
17. S. Barthelmy *et al*., "GRB Coordinates Network (GCN): A Status Report", in *Gamma-Ray Bursts*, eds. R. M. Kippen, R. S. Mallozzi & G. J. Fishman, 731, AIP, New York, 2000.
18. L. Piro *et al.*, "Observation of X-ray Lines from a Gamma-Ray Burst (GRB 991216): Evidence of Moving Ejecta from the Progenitor", *Science*, **290**, 955-958, 2000.
19. J. Reeves *et al*., "The Signature of Supernova Ejecta in the X-ray Afterglow of the γ-ray Burst 011211", *Nature*, **416**, 512-515, 2002.